JCAMECH

Vol. 47, No. 1, June 2016, pp 25-34
DOI: 10.22059/jcamech.2016.59252

From Passive Dynamic Walking to Passive Turning of Biped walker

M. R. Sabaapour[1,*], M. R. Hairi Yazdi[1], B. Beigzadeh[2]

[1]*School of Mechanical Engineering, University of Tehran, Iran*

[2]*Department of Mechanical Engineering, Iran University of Science and Technology, Iran*

Received: 1 Jan. 2016 , Accepted: 2 Apr. 2016

Abstract

Dynamically stable biped robots mimicking human locomotion have received significant attention over the last few decades. Formerly, the existence of stable periodic gaits for straight walking of passive biped walkers was well known and investigated as the notion of passive dynamic walking. This study is aimed to elaborate this notion in the case of three dimensional (3D) walking and extend it for other maneuvers, specifically curved walking or turning. For this purpose, the motion of a general 3D compass gait model on a ramp has been analyzed theoretically in detail. A comprehensive dynamic modeling with respect to the vertical fixed frame is used based on Lagrangian and augmented methods. In addition to 3D passive straight walking, the results confirm the existence of some passive turning motions for the biped walker towards the steepest decent of the ramp. It was shown that the value of passive turning is strictly concerned to the value of initial perturbed condition of the walker, especially to the value of heading angle. A parameter analysis was also accompanied to examine the change in the characteristics of such passive motions caused by the change in model parameters.

Keywords:

3D Biped Robot, Passive walking, Curved walking, Turning, Steering, Asymptotical Stability.

1. Introduction

Efforts to empower biped robots, has resulted in increasing the degrees of actuation as well as the complexity of control strategies [1]. Some researchers sought to minimize this complexity through tracing passive dynamic motions like human beings. McGeer [2] was the first researcher who studied the notion of passive dynamic walking in detail. He showed that a bipedal walker can walk down dynamically stable on a mild slope, without any control input or actuation, just due to gravity.

* Corresponding Author. Tel.: +98 216 119916; Fax: +98 218 8013029
Email Address: sabaapour@ut.ac.ir

McGeer pioneered his work via some basic two dimensional (2D) models, but his attempts to derive a stable 3D case failed because of lateral instability of the model [3]. Coleman et. al. [4] showed that a 3D compass gait model which is supplemented by special moments of inertia as well as arc feet can exhibit stable passive straight walking. Moreover, control of biped robots based on such asymptotical stable periodic gaits or limit cycles was followed in other researches like [5, 6]. However, all of these works were limited to "straight walking".

One of the essential maneuvers that can be considered for a biped walker is curved walking or turning. Statistics shows that 20 to 50 percent of daily walking of human beings include turning [7]. However, so far only few researches have addressed this type of motion for biped robots, especially for the aforementioned asymptotical stable robots [8-13]. This little number of works is also restricted to the study of active models.

The current study aims to elaborate and extend the notion of passive 3D walking for "passive curved walking or turning" which can be based to develop an asymptotically stable steering mechanism of biped robots, with inherent efficiency and natural-looking. To this end, passive turning motions of the simplest bipedal walking model, i.e. "3D rimless spoked wheel" have been well addressed by the authors in some earlier papers [14, 15]. In the present paper, a "3D compass gait biped model" which is more resembled to human than the rimless wheel will be studied. Hence, giving more details about its 3D passive straight walking, we also investigate the possibility of passive curved walking and their features for the new model.

In this regard, the only related work has been probably reported by Wisse et al [16, 17] during experiment on Delft biped robot. They found out if the robot has a special design of a tilted ankle joint which couples the sagittal and frontal dynamics of the robot (like that exists in a skateboard or bicycle), a sideways fall could be averted by a natural passive turning in that direction.

Now, in this paper, not only we investigate this maneuver theoretically, but also we show that it is not restricted to a special design of biped walker considered by them. In another word, we will explain that any general biped walker like the model understudy could exhibit a dynamically stable passive turning mechanism caused by an inherent dynamic coupling between the sagittal and frontal planes.

It is worth to note that, for the goal of this research, the model should be analyzed in a new general framework with respect to the vertical fixed frame. It is especially essential for evaluation of infinite circular turnings in the future.

Hence, the paper is organized as follows: The model and its general equations of motion are first described. Since it is a hybrid system with impact events, the method of Poincare map is applied to find periodic motions and stability analysis. Next, 3D passive straight walking and finite passive turning motions are investigated in detail. Finally, a discussion including parameter analysis is presented. The details of equations of motion are mentioned in appendix.

2. Model description

The 3D biped walker of interest is illustrated in Figure (a). It is a rigid body compass like biped walker composed of two symmetrical straight legs of length l which are connected with a hip joint of width w. The legs are also equipped by two arc-shaped feet of radius R. Each leg has mass m with inertia matrix $\mathbf{I} = [I_{ij}]_{3\times3}$ described at its Center Of Mass (COM). Also this COM is located on $[x_{cm}, y_{cm}, z_{cm}]$ with respect to the body coordinate attached to the lowest point of the leg.

The model is considered to walk on a ramp of angle α passively, just under the action of gravity. According to Figure 1(b), it can be totally identified by four degrees of freedom (DOF) with respect to the vertical fixed frame (XYZ). Three DOFs express yaw-roll-pitch angles of the stance leg i.e. $[\varphi, \psi, \theta]$ respectively, while one additional DOF, θ_{sw}, indicates the relative pitch angle of swing leg with respect to the stance leg. Therefore, the generalized coordinate vector of the model can be totally expressed by

$$\mathbf{q} = [\varphi, \psi, \theta, \theta_{sw}]^{\mathrm{T}} \tag{1}$$

Note that the translation of the model is just a dependent motion relying on the no slip assumption for the rolling on the stance foot (some non-holonomic constraints). For simplicity in results comparison, we tried to take the same parameters as [4], with the exception that our variable angles are measured with respect to the vertical fixed frame (XYZ) whose Z-axis is aligned vertically according to the gravity direction, rather than the normal fixed frame ($X_nY_nZ_n$) whose Z-axis is normal to the ramp. It is essential for later general analysis of the model in terms of 3D turning, especially for the case of infinite or continuous one.

Because our 3D model has a finite hip width, each complete stride consists of two subsequent right and left steps at least. Each step by itself is also composed of two phases of motion described as follows.

Single support or continuous phase: In the

beginning of each step, the model is supported and

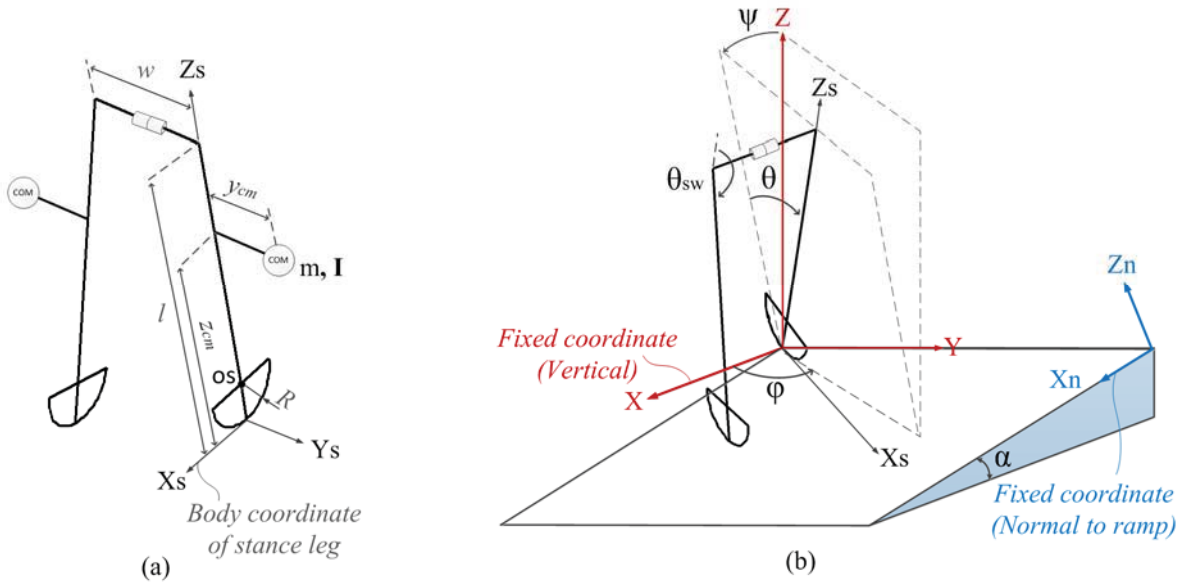

Figure 1: The 3D compass like biped model with finite hip width & arc foot. (a) Parameters definition, (b) DOFs definition

rolled around the one leg (stance leg), while the other leg is moved freely (swing leg). Dynamics of this phase has a continuous nature and can be determined via a constrained Lagrangian method for instance.

Double support or collision phase: Once the swing foot reaches the ground, the next stage is happened. It is assumed that this phase is an instantaneous perfectly plastic collision. The transition rule between two sets of generalized coordinate rates -immediately before and immediately after collision- can be determined straightforward via the method mentioned in [18]. Moreover a resetting rule is needed to relabel stance and swing feet variables conversely at the end of each step. Combination of two rules above gives a general map of this phase.

The details of the equations of motion are presented in Appendix. In conclusion, the model is a hybrid one that can be integrated numerically for each step and expressed in the state form as below

$$\begin{cases} \dot{\mathbf{x}} = \mathbf{f}(\mathbf{x}) & \mathbf{x} \notin \boldsymbol{\mathcal{S}} \quad : \textit{continuous phase} \\ \mathbf{x}^{+} = \Delta(\mathbf{x}^{-}) & \mathbf{x} \in \boldsymbol{\mathcal{S}} \quad : \textit{collision phase} \end{cases} \quad (2)$$
$$= \begin{bmatrix} \mathbf{q} \\ \dot{\mathbf{q}} \end{bmatrix}$$

The vector $\mathbf{x}$ indicates the state vector of the system. The switching surface $\boldsymbol{\mathcal{S}}$ represents a hyper plane in the state space and implies the collision condition in reality (for more details, please refer to appendix)

One of the prevalent method for finding periodic gaits of such hybrid system is the method of Poincare´ map [10]. A *Partial Poincare map* can be defined by a map $\mathbf{P_i}(.)$, that relates the states of the system just after a collision , ${}^{k}\mathbf{x}^{+}$, to just after the next one , ${}^{k+1}\mathbf{x}^{+}$, namely

$${}^{k+1}\mathrm{x}^{+} = \mathrm{P_i}({}^{k}\mathrm{x}^{+}) \quad (3)$$

Consequently, a (complete-*stride) Poincare map* is a composition of the two partial maps above, in relation to two subsequent right and left steps, and can be expressed by $\mathbf{P}(.) = \mathbf{P}_2(\mathbf{P}_1(.))$ as

$${}^{k+2}\mathbf{x}^{+} = \mathbf{P}({}^{k}\mathbf{x}^{+}) \quad (4)$$

Any fixed point of this map, that is any roots of $\mathbf{x}^{*} = \mathbf{P}(\mathbf{x}^{*})$, corresponds to a periodic motion or limit cycle of the system. At this situation, the state of the system returns to its initial value after two successive steps and continues so on. Therefore to find the periodic motions, the following equation can be solved numerically

$$\mathbf{x}^{*} - \mathbf{P}(\mathbf{x}^{*}) = \mathbf{0} \quad (5)$$

Also regarding stability evaluation, if the Jacobian of the map in the neighbourhood of a fixed point has eigenvalues inside the unit circle, we conclude that it is an asymptotically stable fixed point representing a stable periodic motion.

3. Passive Straight Walking

For instance, the parameters of the model are

considered as Table 1. In order to simplify the comparison and generalize the results, all parameters are presented in their dimensionless form using the basic parameters of the leg i.e. length l, mass m, and time $\sqrt{l/g}$.

Table 1: Parameters used for simulation (non-dimensionalized)

R	w	x_{cm}	y_{cm}	z_{cm}	I_{XX}	I_{YY}	I_{ZZ}	I_{XY}	I_{XZ}	I_{YZ}
0.1236	0.3624	0	0.6969	0.3137	0.1982	0.0186	0.1802	0.0071	-0.0023	0.0573

The walker is considered on a ramp of angle $\alpha = 0.0702$. Solving Eq. (5) using a numerical optimization method, one can find a fixed point corresponding to a passive 3D straight walking as below

$$\mathbf{x}^* = \left[\varphi^*, \psi^*, \theta^*, \theta_{sw}^*, \dot{\varphi}^*, \dot{\psi}^*, \dot{\theta}^*, \dot{\theta}_{sw}^*\right]^{\mathrm{T}} = [0.09907, -0.00232, -0.09031, 3.43583, -0 \quad (6)$$

that is represented just after collision of the left foot. The velocity values are written non-dimensional in accordance with the non-dimensional time $\tau = t\sqrt{g/l}$. The simulation results over a gait cycle or one stride of this periodic motion are demonstrated through Figure 2 to Figure 5. Also, the Jacobian analysis of Poincare map about this fixed point confirms the asymptotical stability of its periodic motion. As can be seen in Table 2, the maximum eigenvalue of this case is less than unity, i.e. $|\lambda_{\max}| = 0.7240 < 1$.

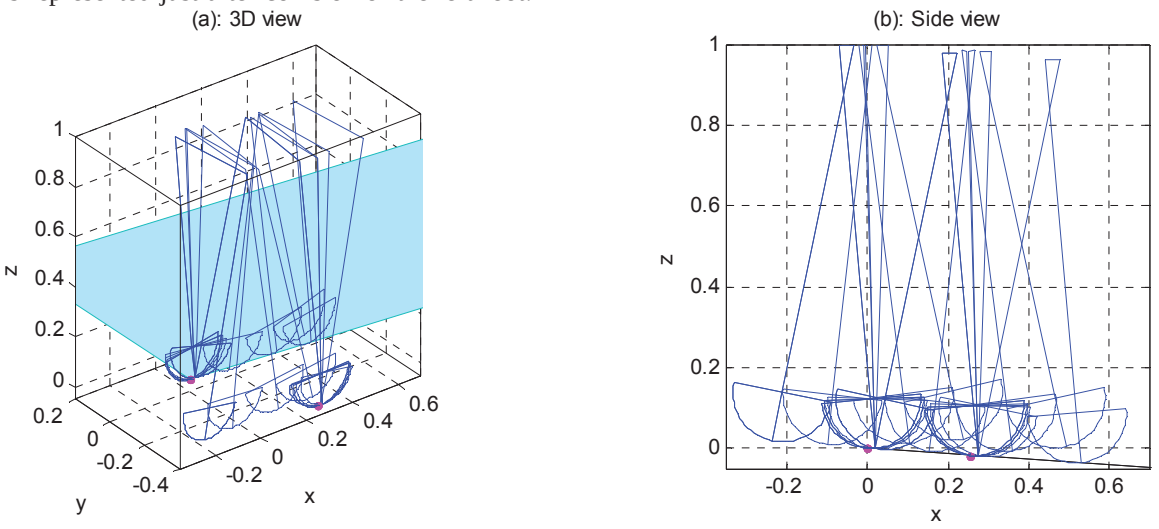

Figure 2: Stick diagram over a gait cycle or stride (two steps) for passive 3D straight walking. X, Y and Z are represented non-dimensional in terms of the leg length, $\boldsymbol{l}$, of the walker.

4. Passive Curved Walking or Turning

Here, we focus on another type of motion which is the final goal of the current study, namely passive curved walking or turning. Roughly speaking, we show that this kind of motion can be realized when the model takes an initial state perturbed than the fixed point of previous straight walking; for example, an initial heading angle not directed to the steepest decent of ramp. At these situations, the walker turns incrementally towards the steepest decent of ramp until becomes parallel to it and then follows aforementioned straight walking. Hence, it can be said that that such passive turnings happen in the basin of attraction of the passive straight walking. This behavior is evaluated more through several simulations as follows.

Let's assume a perturbed initial condition as

$$\mathbf{x}_0 = \mathbf{x}^* + \boldsymbol{\delta}\mathbf{x} = \left[\underbrace{0.09907 + \delta\varphi}_{\varphi_0}, -0.00232, -0.09031, 3.435 \quad (7)$$

which differs from the aforementioned fixed point in terms of the value of heading angle. For instance, in the case of $\varphi_0 = \frac{5\pi}{80} > \varphi^* = 0.09907$, simulation results over 80 steps are shown in Figure 6 to Figure 7. The walker exhibits a finite passive turning until it takes a direction parallel to the steepest descent and walks straightly on the ramp again. Intuitively, it can be said that an initial heading angle other than φ^*, induces a lean angle asymmetry with respect to the

vertical gravity plane. This asymmetry acts as a mass offset and forces the walker to turn passively towards the vertical gravity plane

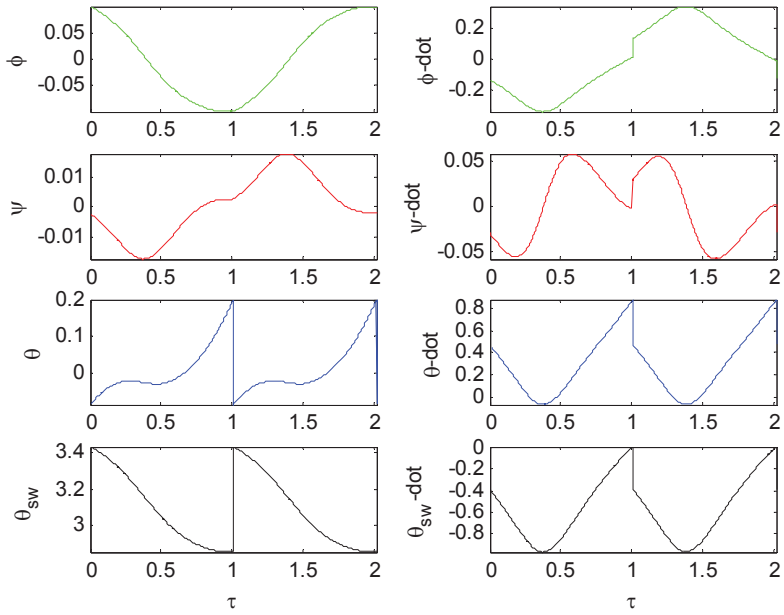

Figure 3: State variables over two steps of passive 3D straight walking. Horizontal axes represent non-dimensional time τ.

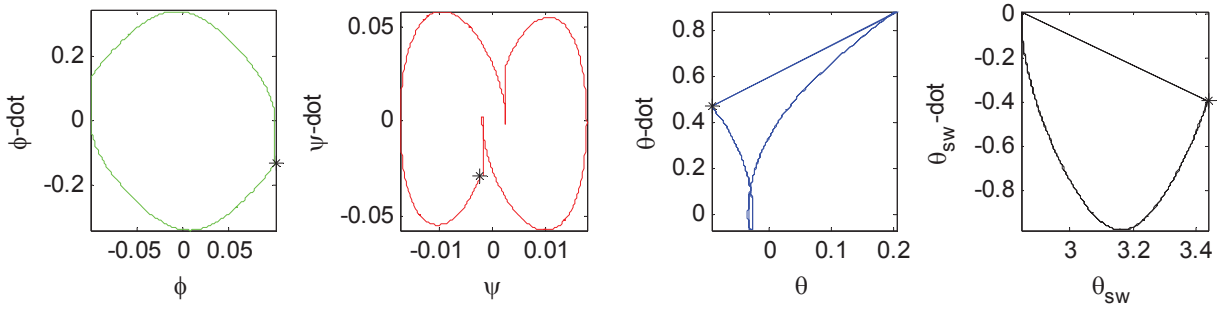

Figure 4: Phase plots over a gait cycle (two steps) of passive 3D straight walking.

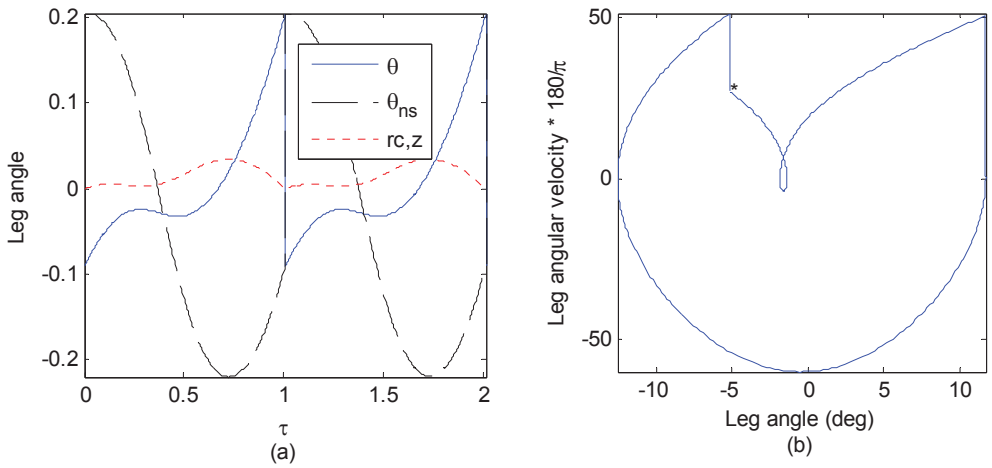

Figure 5: over two steps of passive 3D straight walking: (a) Time plot of leg angles with respect to absolute vertical axis, i.e. $\boldsymbol{\theta}$ for the stance leg & $\boldsymbol{\theta_{ns}} = (\boldsymbol{\theta} + \boldsymbol{\theta_{sw}}) - \boldsymbol{\pi}$ for the swing leg; in addition to distance of swing foot with respect to ground, i.e. $r_{c,z}$. (b) phase portrait corresponding each leg

Table 2: Eigenvectors and eigenvalues of Jacobian matrix about the mentioned fixed point related to 3D straight walking

	Mode I	Mode II	Mode III	Mode IV	Mode V
$\varphi - \varphi^*$	0.0523	-0.0772 +- 0.0556i	0.0953 -+ 0.1768i	0.1670 -+ 0.3858i	0.0246
$\psi - \psi^*$	0.0115	0.0253 -+ 0.0321i	0.1410 +- 0.0216i	0.1402 +- 0.0004i	-0.0506
$\theta - \theta^*$	-0.189	0.1605 -+ 0.1378i	0.2613 +- 0.0568i	0.2462 +- 0.0455i	-0.0985
$\theta_{sw} - \theta^*_{sw}$	0.1574	-0.2549 +- 0.1890i	-0.1584 -+ 0.0165i	-0.1447 -+ 0.0086i	0.0539
$\dot{\varphi} - \dot{\varphi}^*$	0.2229	0.2754 -+ 0.0010i	0.2807 +- 0.0778i	0.2791 +- 0.1032i	-0.2896
$\dot{\psi} - \dot{\psi}^*$	0.0883	-0.0063 -+ 0.0211i	0.0565 +- 0.0265i	0.0582 +- 0.0146i	-0.053
$\dot{\theta} - \dot{\theta}^*$	0.6449	0.0974 -+ 0.0929i	0.3689 -+ 0.0119i	0.3338 -+ 0.0354i	-0.4242
$\dot{\theta}_{sw} - \dot{\theta}^*_{sw}$	0.6807	0.8657 +- 0.0000i	0.7858 +- 0.0000i	0.7858 +- 0.0000i	-0.8471
λ_i	-0.0000+0.0000i	-0.2031 + 0.4490i	0.5344 + 0.4005i	0.6589 + 0.3000i	0.0504+0.0000i
$\lvert\lambda_i\rvert$	0.0000	0.4928	0.6678	0.7240	0.0504

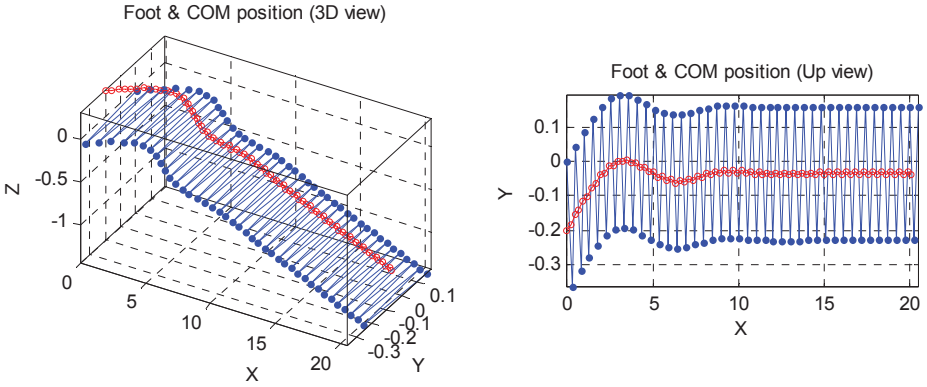

Figure 6: Foot contact and COM position (shown by '.' and 'o' at every step beginning respectively) during a passive turning induced by a perturbed heading angle $\boldsymbol{\varphi_0 = \frac{5\pi}{80}}$. X, Y and Z are represented non-dimensional in terms of the leg length, $\boldsymbol{l}$, of the walker.

Furthermore, different passive turnings caused by different initial heading angles are compared together in Figure 8. Note that 3D straight walking is shown as case I for comparison. Clearly more disturbed initial heading angle yields more finite passive turning.

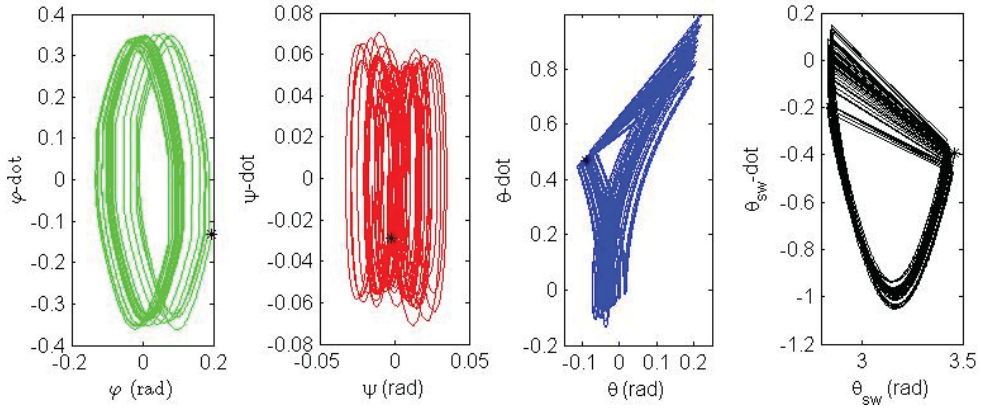

Figure 7: phase plots of a passive turning ($\boldsymbol{\varphi_0 = \frac{5\pi}{80}}$). Initial points are specified by '*'.

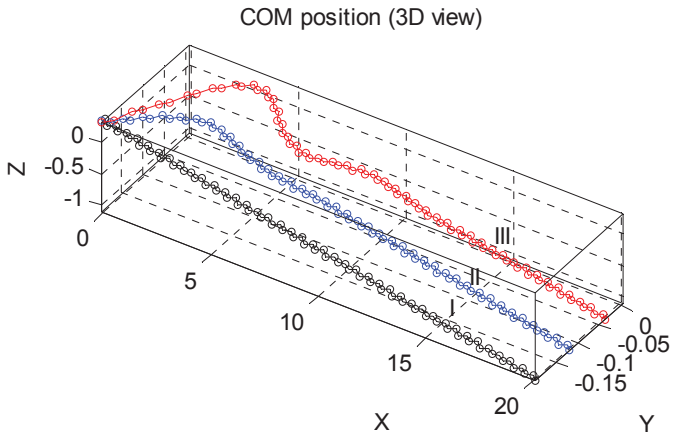

Figure 8: Comparison of COM positions for different initial heading angle resulting different passive turnings. $\boldsymbol{\varphi_{0,I} = \varphi^* < \varphi_{0,II} = \frac{4\pi}{80} < \varphi_{0,III} = \frac{5\pi}{80}}$. X, Y and Z are represented non-dimensional in terms of the leg length, $\boldsymbol{l}$.

5. Discussion

Although the turning motion discussed in this paper could be viewed as a transient phase of a system with stable

behavior, what happens in reality is a kind of non-straight (curved) walking. This give us an inspiration that If we aim at designing an active walking system capable of following curved paths according to the behavior of the passive mechanism, it is sufficient to enter the active stable system into a virtual transient phase (still in domain of attraction), something like the present one. Moreover, it is deduced from the current discussion that if the ramp is not constantly unidirectional, the transient phase could continuously extend. That is, we could construct a system which forces the passive walker to follow a predefined arbitrary curve. For example, to force the passive walker to follow a circular path, the direction of the ramp should change in such a way accordingly. Having constructed such passive walker, the approach to deal with an active robot will be straightforward.

To give more insight into the characteristics of such 3D passive motions, the effects of some model parameters variation are examined here. To this end, the parameters of the model introduced before in Table 1 are assumed again as a basis and specified here by subscript '2'. For instance, the effect of hip width is examined through Table 3 and Figure 9. In another world, different values of hip width are considered for the model whereas all other parameters are held unchanged. The related fixed points and maximum eigenvalues for each case are illustrated in Table 3. Referring to the maximum eigenvalues, it can be said that increasing hip width, firstly improves asymptotical stability of 3D passive walking, although this stability is violated later. Remember that the asymptotical stability of a periodic motion increases as the maximum eigenvalue is kept away from unity more in magnitude. Furthermore, a perturbed motion started from a perturbed initial heading angle of $\varphi_0 = 7\pi/160$ is simulated for each case and compared in Figure 9. As we expected, all of them represent a same value of passive turning, but with different oscillatory behaviors in accordance with their different stability characteristics specified before.

Table 3: Different fixed points of 3D passive straight walking related to different model hip width (shown up to order 10^{-5})

	φ^*	ψ^*	θ^*	θ^*_{sw}	$\dot{\varphi}^*$	$\dot{\psi}^*$	$\dot{\theta}^*$	$\dot{\theta}^*_{sw}$	$\lvert\lambda_{max}\rvert$
$w_1 = 0.32616$	0.10110	-0.00149	-0.08913	3.43793	-0.13168	-0.02474	0.47311	-0.39098	0.9596
$w_2 = 0.3624$	0.09907	-0.00232	-0.09031	3.43583	-0.13050	-0.02909	0.47124	-0.39256	0.7240
$w_3 = 0.39864$	0.09694	-0.00306	-0.09138	3.43329	-0.12924	-0.03309	0.46887	-0.39384	0.7949

Also a similar comparison about the effect of arc foot can be performed as illustrated in Table 4 and Figure 10. However, its effect on the stability is similar to that of the hip width.

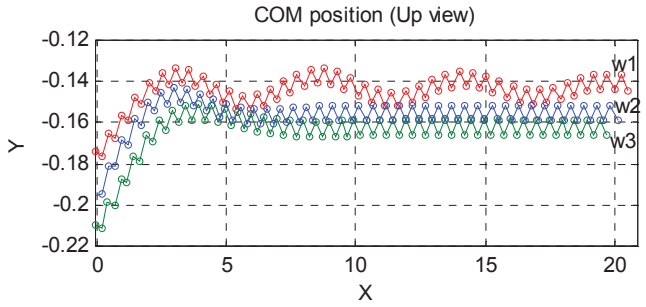

Figure 9: Comparison of different passive turnings related to different model hip width ($\mathbf{w1 < w2 < w3}$), but a same initial heading angle ($\boldsymbol{\varphi_0 = \frac{7\pi}{160}}$). X and Y are represented non-dimensional in terms of the leg length, $\boldsymbol{l}$.

Table 4: Different fixed points of 3D passive straight walking related to different model arc foot (shown up to order 10^{-5})

	φ^*	ψ^*	θ^*	θ^*_{sw}	$\dot{\varphi}^*$	$\dot{\psi}^*$	$\dot{\theta}^*$	$\dot{\theta}^*_{sw}$	$\lvert\lambda_{max}\rvert$
$R_1 = 0.0618$	0.08705	-0.00278	-0.07235	3.39952	-0.10426	-0.03569	0.43501	-0.31109	0.8227
$R_2 = 0.1236$	0.09907	-0.00232	-0.09031	3.43583	-0.13050	-0.02909	0.47124	-0.39256	0.7240
$R_3 = 0.14832$	0.10446	-0.00209	-0.09838	3.45215	-0.14158	-0.02615	0.48824	-0.42731	0.9024

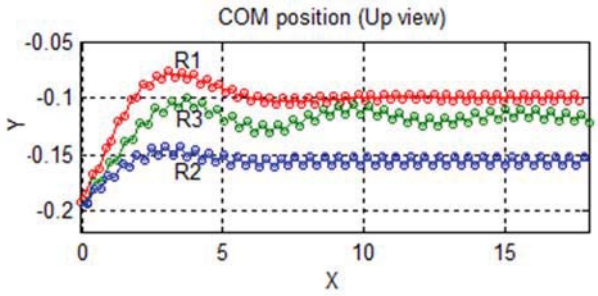

Figure 10: Comparison of different passive turnings related to different model arc foot ($\mathbf{R1 < R2 < R3}$), but a same initial heading angle ($\boldsymbol{\varphi_0 = \frac{7\pi}{160}}$)

6. Conclusion

This paper investigated the concept of passive straight walking in three-dimensional space and introduced an extension, namely "passive curved walking or turning". To this end, a general 3D compass-gait biped model with arc feet was considered. A new extendable dynamic model was proposed with respect to a general vertical fixed frame. Using this model, 3D passive straight walking was evaluated more precisely as well as a new category of passive maneuvers namely passive turning was studied. It was shown that the value of passive turning is strictly concerned to the value of initial perturbed condition from passive straight walking, especially in terms of heading angle. It was highlighted that increasing hip width or foot radius firstly increases asymptotical stability, but shows instability effects thereafter. Future works include exploiting the results of "finite passive turning" presented in this work to develop a set of "infinite passive turning" motions and consequently an efficient, natural-looking steering mechanism.

7. Appendix

The details of equations of motion are presented here. Since the motion is governed by some non-holonomic constraints, three additional generalized coordinates specifying the model translation are also applied such that the extended or dependent generalized coordinate vector could be considered as

$$\mathbf{q_e} = [\mathbf{q^T}, X_{os}, Y_{os}, Z_{os}]^{\mathrm{T}} \tag{A1}$$

where $[X_{os}, Y_{os}, Z_{os}]$ represents the position vector of stance foot arc center with respect to the global vertical fixed frame. Now we can apply the Lagrange multipliers technique as follows.

7.1. *Single support phase:*

Applying the Lagrange equations, one can derive equations of motion in the standard form below

$$\mathbf{M_e}(\mathbf{q_e})\ddot{\mathbf{q}}_\mathbf{e} + \mathbf{V_e}(\mathbf{q_e}, \dot{\mathbf{q}}_\mathbf{e}) = \mathbf{Q_e} := \mathbf{E}^T\,\boldsymbol{\lambda} \tag{A2}$$

where $\mathbf{Q_{e_{7\times1}}}$ represents the vector of generalized external forces acting on the robot, $\boldsymbol{\lambda_{3\times1}}$ indicates three unknown Lagrange multipliers related to three

physically meaningful forces at the contact point, and also matrix $\mathbf{E_{3\times 7}}$ is defined as $\mathbf{E} \coloneqq \partial\, \boldsymbol{\delta}\mathbf{r_c}/\, \partial \mathbf{q_e}$, in witch $\mathbf{r_c}$ denotes the position vector of the contact point between stance foot and the ground. Moreover, constraint equations for no slip rolling of stance foot can be expressed as

$$\mathbf{v_c} \coloneqq \mathbf{E}\dot{\mathbf{q}}_\mathbf{e} = \mathbf{0} \tag{A3}$$

The seven equations in Eq. (A2) and the three constraint equations above can be used together to solve for the ten unknowns, i.e. $\ddot{\mathbf{q}}_\mathbf{e}$ and $\boldsymbol{\lambda}$. To do so, one can differentiate constraint equations and apply an augmented form as

$$\begin{bmatrix} \mathbf{M_{e}}_{7\times 7} & -\mathbf{E}^{\mathbf{T}}{}_{7\times 3} \\ -\mathbf{E_{3\times 7}} & \mathbf{0_{3\times 3}} \end{bmatrix} \begin{bmatrix} \ddot{\mathbf{q}}_\mathbf{e} \\ \boldsymbol{\lambda} \end{bmatrix} = \begin{bmatrix} -\mathbf{V_e} \\ \dot{\mathbf{E}}\dot{\mathbf{q}}_\mathbf{e} \end{bmatrix} \tag{A4}$$

Once this is solved numerically, $\ddot{\mathbf{q}}$ and consequently $\mathbf{x} = [\mathbf{q}^\mathbf{T}\ \dot{\mathbf{q}}^\mathbf{T}]^\mathbf{T}$ will be in hand. It should be reminded that the equations of motion for this stage are finally interpreted in the state space form as

$$\dot{\mathbf{x}} = \mathbf{f}(\mathbf{x}) \coloneqq \begin{bmatrix} \dot{\mathbf{q}} \\ \mathbf{M^{-1}}(\mathbf{Q} - \mathbf{V}) \end{bmatrix} \tag{A5}$$

7.2. *Double support or collision phase:*

For the collision phase, the procedure mentioned in [18] can be used. Assuming equations of motion similar to Eq. (A1) and then integrating them over the duration of collision (t^- to t^+), one can obtain

$$\mathbf{M_e}(\dot{\mathbf{q}}_\mathbf{e}^+ - \dot{\mathbf{q}}_e^-) = \widehat{\mathbb{Q}}_\mathbf{e} \coloneqq \mathbb{E}^\mathbf{T}\hat{\boldsymbol{\lambda}} \tag{A6}$$

where $\widehat{\mathbb{Q}}_e$ represents generalized impacts acting on the robot, $\hat{\boldsymbol{\lambda}}_{\mathbf{3\times 1}}$ indicates three unknown Lagrange multipliers related to three physically impacts at the impact point, and also matrix $\mathbb{E}$ is defined as $\mathbb{E} \coloneqq \boldsymbol{\partial}\, \boldsymbol{\delta}\mathbf{r_{csw}}/\, \boldsymbol{\partial}\mathbf{q_e}$, in which $\mathbf{r_{csw}}$ denotes the position vector of the contact point on the swing foot. For the instant immediately after the collision, we also deal with no-slip constraint for the impact point in the form

$$\mathbf{v}_{\boldsymbol{csw}}^+ \coloneqq \mathbb{E}\dot{\mathbf{q}}_e^+ = \mathbf{0} \tag{A7}$$

So differentiating Equation above and combining with previous Equation, one can obtain

$$\begin{bmatrix} \mathbf{M_{e}}_{7\times 7} & -\mathbb{E}^{\mathbf{T}}{}_{7\times 3} \\ -\mathbb{E}_{3\times 7} & \mathbf{0_{3\times 3}} \end{bmatrix} \begin{bmatrix} \dot{\mathbf{q}}_e^+ \\ \hat{\boldsymbol{\lambda}} \end{bmatrix} = \begin{bmatrix} \mathbf{M_e}\dot{\mathbf{q}}_e^- \\ \mathbf{0} \end{bmatrix} \tag{A8}$$

Solving this equation, the unknowns such as $\dot{\mathbf{q}}^+$ can be found readily. It is known that the stance and swing legs must be relabeled at the end of each step. For this purpose, $\mathbf{q}^+$ (and subsequently $\dot{\mathbf{q}}^+$) are reset by way of

$$\begin{bmatrix} \varphi \\ \psi \\ \theta \\ \theta_{sw} \\ \mathrm{X_{os}} \\ \mathrm{Y_{os}} \\ \mathrm{Z_{os}} \end{bmatrix}^+ = \begin{bmatrix} \varphi \\ \psi \\ -\big(\pi - (\theta + \theta_{sw})\big) \equiv -\theta_{ns} \\ 2\pi - \theta_{sw} \equiv -\theta_{sw} \\ \mathrm{X_{osw}} \\ \mathrm{Y_{osw}} \\ \mathrm{Z_{osw}} \end{bmatrix}^- \tag{A9}$$

reminding the perfectly plastic assumption for the collision. In addition, the sign of parameters w, y, I_{xy} and I_{yz} must be reversed accordingly at the end of each step. In conclusion, a general nonlinear map between the states of this stage can be obtained by combining numerically two set of rules above and interpreted as

$$\mathbf{x}^+ = \Delta(\mathbf{x}^-) \tag{A10}$$

References:

[1] F. Farzadpour, M. Danesh, S. M. TorkLarki, Development of multi-phase dynamic equations for a seven-link biped robot with improved foot rotation in the double support phase, *Proceedings of the Institution of Mechanical Engineers, Part C: Journal of Mechanical Engineering Science*, Vol. 229, No. 1, pp. 3-17, 2015 .

[2] T. McGeer, Passive dynamic walking, *The International Journal of Robotics Research*, Vol. 9, No. 2, pp. 62-82, 1990 .

[3] T. McGeer, Passive dynamic biped catalogue, in *Proceeding of Experimental Robotics II: The 2nd International Symposium*, Springer-Verlag, pp. 463-490, 1991 .

[4] M. J. Coleman, M. Garcia, K. Mombaur, A. Ruina, Prediction of stable walking for a toy that cannot stand, *Physical Review E*, Vol. 64, No. 2, pp. 022901, 2001 .

[5] A. Goswami, B. Thuilot, B. Espiau, Compass-like biped robot part I: Stability and bifurcation of passive gaits, 1996 .

[6] M. W. Spong, Passivity based control of the compass gait biped, in *Proceeding of IFAC World Congress*, Citeseer, pp. 19-24, 1999 .

[7] M. S. Orendurff, A. D. Segal, J. S. Berge, K. C. Flick, D. Spanier, G. K. Klute, The kinematics and kinetics of turning: limb asymmetries associated with walking a circular path, *Gait & Posture*, Vol. 23, No. 1, pp. 106-111, 2006 .

[8] R. D. Gregg IV, *Geometric control and motion planning for three-dimensional bipedal locomotion*, Ph.D. Thesis, Electrical & Computer Engr, University of Illinois at Urbana-Champaign, 2011 .

[9] R. D. Gregg, A. K. Tilton, S. Candido, T. Bretl, M. W. Spong, Control and Planning of 3D Dynamic

Walking with Asymptotically Stable Gait Primitives, 2012 .

[10] C. Shih, J. Grizzle, C. Chevallereau, Asymptotically stable walking and steering of a 3D bipedal robot with passive point feet, *IEEE Transactions on Robotics*, 2009 .

[11] S. Lim, Y. I. Son, Discrete-Time Circular Walking Pattern for Biped Robots, *Journal of Electric Engineering Technology*, Vol. 2, No. 2, pp. 2, 2016 .

[12] Y. Cao, S. Suzuki, Turn Control of a Three-Dimensional Quasi-Passive Walking Robot by Utilizing a Mechanical Oscillator, *Engineering*, Vol. 6, pp. 93-99, 2014 .

[13] F. Ikeda, S. Toyama, A proposal of right and left turning mechanism for quasi-passive walking robot, in *Proceeding of International Conference on Advanced Robotics and Intelligent Systems (ARIS) 2015*, 1-5, 2015 .

[14] M. R. Sabaapour, M. R. Hairi-Yazdi, B. Beigzadeh, Towards Passive Turning in Biped Walkers, *Procedia Technology*, Vol. 12, No. 0, pp. 98-104, 2014 .

[15] M. R. Sabaapour, M. R. Hairi-Yazdi, B. Beigzadeh, Passive Turning Motion of 3D Rimless Wheel: Novel Periodic Gaits for Bipedal Curved Walking, *Advanced Robotics*, 2015 .

[16] M. Wisse, Three additions to passive dynamic walking; actuation, an upper body, and 3D stability, in *Proceeding of 2004 4th IEEE/RAS International Conference on Humanoid Robots*, IEEE, pp. 113-132, 2004 .

[17] M. Wisse, R. Q. van der Linde, 2007, *Delft pneumatic bipeds*, Springer Berlin Heidelberg, Germany

[18] J. W. Grizzle, G. Abba, F. Plestan, Asymptotically stable walking for biped robots: Analysis via systems with impulse effects, *Automatic Control, IEEE Transactions on*, Vol. 46, No. 1, pp. 51-64, 2001 .